Communications in Physics, Vol. 32, No. 4 (2022), pp. 401-412
DOI: https://doi.org/10.15625/0868-3166/16890

ANALYSIS OF TEMPERATURE-DEPENDENT EXTENDED X-RAY ABSORPTION FINE STRUCTURE OSCILLATION OF DISTORTED CRYSTALLINE CADMIUM

TONG SY TIEN†

Department of Basic Sciences, University of Fire Prevention and Fighting, 243 Khuat Duy Tien, Thanh Xuan, Hanoi 120602, Vietnam

E-mail: †tongsytien@yahoo.com

Received 22 January 2022
Accepted for publication 1 July 2022
Published 22 September 2022

Abstract. *In this paper, the temperature-dependent extended X-ray absorption fine structure (EXAFS) of distorted crystalline cadmium has been analyzed using an efficient calculation-model. The analysis procedure is based on evaluating the influence of temperature on the phase shift and amplitude reduction of EXAFS oscillation that is expressed in terms of the EXAFS Debye-Waller factor. The anharmonic EXAFS cumulants are calculated by expanding the anharmonic correlated Debye model based on the anharmonic effective potential that depends on the structural characteristics of distorted crystalline cadmium. The numerical results satisfy well with those obtained using the experimental data and other models at various temperatures. The obtained results indicate that this theoretical model is useful for calculating and analyzing the experimental EXAFS data of distorted crystalline metals.*

Keywords: crystalline cadmium; anharmonic correlated Debye model; Debye-Waller factor; EXAFS oscillation.

Classification numbers: 65.20.+w; 78.90.+t.

I. INTRODUCTION

Nowadays, the extended X-ray absorption fine structure (EXAFS) technique is a widely employed probe of the dynamical behaviors and structural parameters in disordered systems [1,2]. This is because EXAFS spectroscopy can contain information about local structures around X-ray absorbing atoms and gives interatomic distances and coordination numbers in crystal lattices [3,4]. This resulted in the EXAFS technique being developed and expanded greatly based on the rapid

development of synchrotron radiation facilities worldwide [5–7]. In reality, thermal disorders are very sensitive to EXAFS oscillation under the influence of temperature because these disorders can disturb the arrangement of atoms in the crystal lattice [7, 8]. The temperature-dependent EXAFS oscillation can be described using a cumulant expansion approach proposed by Bunker, in which the anharmonic EXAFS oscillation is presented in terms of the Debye-Waller (DW) factor via the power moments of radial pair distribution (RD) function [9, 10]. In this approach, the thermodynamic properties and structural parameters of materials can easily be derived using the IFEFFIT program suite [11, 12] based on fitting the experimental EXAFS signals with a theoretical EXAFS oscillation [13, 14]. Therefore, to obtain reliable results, it needs suitable physical approximations and theoretical models that can accurately describe the anharmonic EXAFS DW factor implemented in the FEFF code of this program suite [15, 16].

In recent years, crystalline cadmium (Cd) has been widely used to produce many essential materials in emerging technologies, such as rechargeable batteries, colorants, coating layers, metal-plated sheets, heat stabilizers, etc. [17–20]. Compared to other cubic crystals, this crystal has lower symmetry and isotropy because it has a hexagonal close-packed (HCP) structure with a non-ideal axial ratio c/a [18, 19].

The temperature-dependent EXAFS cumulants of Cd have also been obtained from the anharmonic correlated Einstein (ACE) (only the first three cumulants) [21] and classical anharmonic correlated Einstein (CACE) [22] models and experiment [22] by Hung *et al*. (2008,2014). However, the ACE and CACE models have not yet evaluated the influence of cumulants on the anharmonic EXAFS oscillation in detail. And only the first three cumulants are calculated in the ACE model, and the CACE is not valid at the low-temperature (LT) region. Also, these models use an ideal axial ratio $c/a \approx \sqrt{8/3}$ in calculations, so Cd is only approximated as an undistorted crystal [21, 22]. It means that the previous works have not considered the effect of structural distortions on the anharmonic EXAFS oscillation of Cd.

Moreover, the effect of structural distortion on the anharmonic EXAFS signals has been discussed by Tien in recent works [3, 5, 16]. The initial obtained results have shown that ignoring this effect can lead to non-negligible errors in the experimental EXAFS data analysis of distorted crystals. However, these works have not fully evaluated the effect of structural distortions on the temperature-dependent EXAFS oscillation, and Cd with a distorted structure has also not been considered in these investigations.

Recently, an anharmonic correlated Debye (ACD) model was efficiently applied in investigating the temperature-dependent EXAFS oscillation of many metals [23–26]. The advantage of this model is that it can calculate all first four cumulants and is valid even in the LT region for crystals that have multiple acoustic phonons with low symmetry and isotropy. Therefore, the analysis and calculation of the temperature-dependent EXAFS oscillation of Cd with a distorted structure is based on the extension of the ACD model, which is a useful addition to the analysis of the experimental data in the advanced EXAFS technique.

II. FORMALISM

K-edge EXAFS function in the framework of plane-wave approximation for one scattering path, including a non-Gaussian disorder, can be expressed via the anharmonic EXAFS cumulants [27–30]:

$$\xi^{(k,T)} \approx \frac{NS_0^2(k)e^{-2R(T)/\lambda(k)}}{(kR(T)^2}F(k)\exp\left\{-2k^2\sigma^2(T)+\frac{2k^4}{3}\sigma^{(4)}(T)\right\} \times \sin\left\{2kr_0+2k\sigma^{(1)}(T)-4k\left[\frac{1}{R(T)}+\frac{1}{\lambda(k)}\right]\sigma^2(T)-(4k^3)/3\sigma^{(}(3))(T)+\delta(k)\right\}, \tag{1}$$

where k is the photoelectron wavenumber, T is the temperature, $\sigma^{(n)}(T)$ is n^{th}-order cumulants, $\lambda(k)$ is the electron mean free path, $F(k)$ is the atomic backscattering amplitude, is the coordination number, $S_0^2(k)$ is the square of the many body overlap term, $\delta(k)$ is the net phase shift, and r_0 and $R(T)$ are the equilibrium distance and the average distance between the absorbing and backscattering atoms, respectively.

The amplitude $A(k,T)$ and phase $\Phi(k,T)$ of K-edge EXAFS function in an expression form $\xi(k,T)=A(k,T)\sin\Phi(k,T)$ can be defined from Eq. (1) as

$$A(k,T)=\frac{NS_0^2(k)}{k}F(k)\exp\left\{-2\ln R(T)-\frac{2R(T)}{\lambda(k)}-2k^2\sigma^2(T)+\frac{2k^4}{3}\sigma^{(4)}(T)\right\}, \tag{2}$$

$$\Phi(k,T)=2kr_0+2k\sigma^{(1)}(T)-4k\left[\frac{1}{R(T)}+\frac{1}{\lambda(k)}\right]\sigma^2(T)-\frac{4k^3}{3}\sigma^{(3)}(T)+\delta(k). \tag{3}$$

Therefore, thermal vibrations influence the K-edge EXAFS amplitude and phase as the temperature changes in the crystal lattice. Assuming that the quantities $S_0^2(k)$, $\delta(k)$, $\lambda(k)$, and $F(k)$ are to be similar at the definite temperatures and reference temperature T_0 [31, 32], the logarithm of amplitude ratio $M(k,T)$ and phase difference $\delta\Phi(k,T)$ between the definite temperatures T and the reference temperature T_0 can be inferred from Eqs. (2) and (3) in the form:

$$M(k,T)=\ln\left[\frac{A(k,T)}{A(k,T_0)}\right]\approx -2k^2\left\{\sigma^2(T)-\sigma^2(T_0)\right\}+\frac{2k^4}{3}\left\{\sigma^{(4)}(T)-\sigma^{(4)}(T_0)\right\}, \tag{4}$$

$$\begin{aligned}\delta\Phi(k,T)=&\Phi(k,T)-\Phi(k,T_0)\\ \approx&2k\left\{\sigma^{(1)}(T)-\sigma^{(1)}(T_0)\right\}\\ &-4k\left\{\frac{1}{r_0}+\frac{1}{\lambda(k)}\right\}\sigma^2(T)-\sigma^2(T_0)-\frac{4k^3}{3}\sigma^{(3)}(T)-\sigma^{(3)}(T_0),\end{aligned} \tag{5}$$

where the contribution of the term $-2\left\{\ln\left[\frac{R(T)}{R(T_0)}\right]+\frac{R(T)-R(T_0)}{\lambda(k)}\right\}$ is considered negligible in Eq. (4), and the approximate expressions $1/R(T)\approx 1/R(T_0)\approx 1/r_0$ are used in Eq. (5).

For cubic metals, the Morse potential can validly determine the pair interaction potential of atoms [33, 34]. If this potential is expanded around its minimum position to the fourth order, it can be written as

$$\Phi(x)=D\left(e^{-2\alpha x}-2e^{-\alpha x}\right)\simeq -D+D\alpha^2x^2-D\alpha^3x^3+7\frac{D\alpha^4x^4}{12}, \tag{6}$$

where m_i is the deviation of the instantaneous bond length between two atoms from equilibrium, D is the dissociation energy, and α characterizes the width of the potential.

In the relative vibrations of backscattering and absorbing atoms, considering only the nearest-neighbor interactions and including the correlation-effect, the anharmonic effective (AE) potential in the center of mass frame of single bond pair of absorber and backscatter atoms is given by [35]

$$V_{eff} = V(x) + \sum_{i=1,2} \sum_{j \neq 1,2} V\left(\varepsilon_i x \hat{R}_{12} \hat{R}_{ij}\right), \varepsilon_i = \mu / m_i, \tag{7}$$

where m_i is the mass of the ith atom, $\mu = m_1 m_2/(m_1 + m_2)$ is the reduced mass of the absorber (1) and backscatter (2), the sum i is the over absorber and backscatter, the sum j is over their nearest neighbor atoms, $\hat{R}_{12}$ is direction unit vector linking absorber and backscatter, and $\hat{R}_{ij}$ is the unit vector along with bond between the i^{th} and j^{th} atoms.

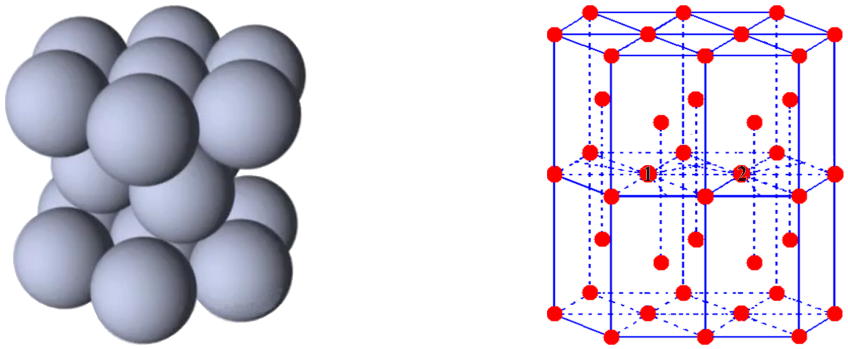

Fig. 1. (a) The crystal model and of Cd with a distorted HCP structure and (b) The schematic diagram of the nearest-neighbor atoms of absorbing and backscattering atoms.

The distorted HCP structure of Cd is shown in Fig. 1(a), and the schematic diagram of the nearest-neighbor atoms of absorbing (1) and backscattering (2) atoms is shown in Fig. 1(b). It can be seen that each atom is similar and is bonded to twelve other surrounding atoms in the first shell. In this crystal, the lattice constants c and a are often used to describe a unit cell, and the distortion-degree of HCP structure can be characterized by the ratio $e = c/a$, in which c is the height, and a is the basal plane edge length. For monatomic crystals like Cd, the values of the parameter are the same, and the values of the parameter in Eq. (7) are all equal $1/2$ because all atoms are the same and have mass $m_i = m$. Herein, in calculating the AE potential $V_{eff}(x)$ from Eq. (7), the structural parameter e appears in the scalar multiplication of the term $\hat{R}_{12}\hat{R}_{ij}$, in which i is the position of absorbing and backscattering atoms, and the sum j is the position of their nearest-neighbor atoms, as seen in Fig. 1(b). Ignoring the overall constant after the use of the Morse potential in Eq. (6) to calculate the AE potential of Cd from Eq. (7), we obtain the result in the form:

$$V_{eff}(x) = \frac{1}{2} k_0 x^2 - k_3 x^3 + k_4 x^4, \tag{8}$$

where k_3 and k_4 are the anharmonic force constants, k_0 is the effective force constant [4, 22], and they can be written in the temperature-independence as follows:

$$k_0 = 4\left(\frac{3e^2+7}{3e^2+4}\right) D\alpha^2,\ k_3 = \frac{5}{4} D\alpha^3,\ k_4 = \frac{7\left(333e^4+888e^2+736\right)}{384(3e^2+4)^2} D\alpha^4. \tag{9}$$

The ACD model is developed from the correlated Debye model using the many-body perturbation (MBP) approach and the AE potential [23–26]. In this model, each atomic vibration in a crystal lattice is quantized as a phonon, and each phonon is treated using a wave described via the dispersion relation:

$$\omega(q) = \omega_D \left|\sin(qa/2)\right|, |q| \leq \pi/a, \tag{10}$$

where $\omega(q)$ is the oscillation frequency, ω_D is the correlated Debye frequency, a is a lattice constant in the one-dimensional system, and q is the phonon wavenumber in the first Brillouin (FB) zone.

In a crystal lattice, the correlated Debye temperatureθ_D and frequency ω_D of Cd can characterize atomic thermal vibrations [24, 25]. They are obtained using the effective force constant from Eq. (9) as follows:

$$\omega_D = 2\sqrt{k_0/m} = 4\alpha\sqrt{\frac{(3e^2+7)D}{3e^2+4)m}},\ \theta_D = \frac{\hbar\omega_D}{k_B} = 4\frac{\hbar\alpha}{k_B}\sqrt{\frac{(3e^2+7)D}{(3e^2+4)m}}, \tag{11}$$

where ω_D can be treated using the formula $\omega_D = cq_D$, k_B is the Boltzmann constant and $\hbar$ is the reduced Planck constant.

The general expressions of the anharmonic EXAFS cumulants in the ACD model were calculated by Hung *et al.* in previous works [23]. However, these obtained expressions are not optimized yet because they still depend on the lattice constant a. Therefore, we have extended the previous ACD model to calculate the temperature-dependent EXAFS cumulants of Cd. After substituting the expressions of local force constants k_0, k_3 and k_4 in Eq. (9) into these general expressions in the ACD model [23] and converting from variable to variable in the formula , we obtain the following results:

$$\sigma^{(1)}(T) = \langle r\rangle - r_0 = \langle x\rangle \frac{15\hbar}{64\pi D\alpha}\left(\frac{(3e^2+4)}{(3e^2+7)}\right)^2 \int_0^{\pi/2} dp \times \omega(p)\frac{1+Z(p)}{1-Z(p)}, \tag{12}$$

$$\sigma^2(T) = \langle (r-R)^2\rangle = \langle x^2\rangle - \langle x\rangle^2 \approx \frac{\hbar}{4\pi D\alpha^2}\left(\frac{3e^2+4}{3e^2+7}\right)\int_0^{\pi/2} dp \times \omega(p)\frac{1+Z(p)}{1-Z(p)}, \tag{13}$$

$$\sigma^{(3)}(T) = \langle (r-R)^3\rangle = \langle x-\langle x\rangle)^3\rangle \approx \frac{5\hbar^2}{64\pi^2D^2\alpha^3}\left(\frac{3e^2+4}{3e^2+7}\right)^3 \int_0^{\pi/2} dp_1 \int_{-\pi/2}^{\pi/2-p_1} dp_2 F(p_1,p_2), \tag{14}$$

$$\sigma^{(4)}(T) = \langle (r-R)^4\rangle - 3(\sigma^2)^2 = \left\langle (x-\langle x\rangle)^4\right\rangle - 3(\sigma^2)^2 \tag{15}$$

$$\approx \frac{21\hbar^3}{\pi^3D^3\alpha^4} \times \frac{(333e^4+888e^2+736)(3e^2+4)^2}{16384(3e^2+7)^4}\int_0^{\pi/2} dp_1 \int_0^{\pi/2-p_1} dp_2 \int_{-\pi/2}^{\pi/2-p_1-p_2} dp_3 G(p_1,p_2),$$

where the angular bracket $\langle\ \rangle$ is the thermal average, $\sigma^{(1)}$ characterizes the net thermal expansion (NTE), $\sigma^{(2)}$ is the parallel mean-square relative displacement (MSRD) σ^2, $\sigma^{(3)}$ is the mean-cubic relative displacement (MCRD), $\sigma^{(4)}$ describes the symmetric deviations from the Gaussian shape,

and the related functions $Z(p)$, $F(p_1,p_2)$, $G(p_1,p_2)$ are identified as

$$Z(p) = \exp\{\beta\hbar\omega(p)\}, \tag{16}$$

$$\begin{aligned} F(p_1,p_2) =& \frac{\omega(p_1)\omega(p_2)\omega(p_1+p_2)}{\omega(p_1)+\omega(p_2)+\omega(p_1+p_2)} \\ &\times\left\{1+6\left(\frac{\omega(p_1)+\omega(p_2)}{\omega(p_1)+\omega(p_2)-\omega(p_1+p_2)}\right.\right. \\ &\left.\left.\times\frac{Z(p_1)Z(p_2)-Z(p_1+p_2)}{[Z(p_1)-1][Z(p_2)-1][Z(p_1+p_2)-1]}\right)\right\}, \end{aligned} \tag{17}$$

$$\begin{aligned} G(p_1,p_2) =& \frac{\omega(p_1)\omega(p_2)\omega(p_3)\omega(p_1+p_2+p_3)}{\omega(p_1)+\omega(p_2)+\omega(p_3)+\omega(p_1+p_2+p_3)} \\ &\times\left\{1+8\left(\frac{Z(p_1)Z(p_2)Z(p_3)-Z(p_1+p_2+p_3)}{[Z(p_1)-1][Z(p_2)-1][Z(p_3)-1][Z(p_1+p_2+p_3)-1]}\right.\right. \\ &\left.\times\frac{\omega(p_1)+\omega(p_2)+\omega(p_3)}{\omega(p_1)+\omega(p_2)+\omega(p_3)-\omega(p_1+p_2+p_3)}\right) \\ &+6\left(\frac{Z(p_1)Z(p_2)-Z(p_3)Z(p_1+p_2+p_3)}{[Z(p_1)-1][Z(p_2)-1][Z(p_3)-1][Z(p_1+p_2+p_3)-1]}\right. \\ &\left.\left.\times\frac{\omega(p_3)+\omega(p_1+p_2+p_3)}{\omega(p_1)+\omega(p_2)-\omega(p_3)-\omega(p_1+p_2+p_3)}\right)\right\}. \end{aligned} \tag{18}$$

Herein, the obtained expressions using the present ACD model are derived from the AE potential. This potential took into account three-dimensional interactions because the second term in Eq. (7) includes the influence of nearest-neighbor atoms on a pair interaction potential. Therefore, in this ACD model, the three-dimensional vibration can be modeled using the one-dimensional vibration model based on the dispersion relation in the crystal lattice. The modeling in the present approach is also used in the previous ACD models and has shown its validity and effectiveness [23–26].

Thus, an extended ACD model can successfully calculate the correlated Debye temperature and frequency, local force constants, and anharmonic EXAFS cumulants of Cd. The obtained expressions of these EXAFS cumulants can satisfy all fundamental properties in their temperature dependence and have also been optimized to not depend on the lattice constant as in the previous ACD model. In this work, the effect of structural distortion is caused by the non-ideal axial ratio of Cd described via a structural parameter e in the calculated expressions. Meanwhile, this effect was not considered in the previous works because Cd is only considered an undistorted crystal using a structural parameter $e \approx \sqrt{8/3}$.

III. NUMERICAL RESULTS AND DISCUSSIONS

To discuss the efficiency of the present theoretical model in calculating and analyzing the temperature-dependent EXAFS oscillation of Cd, we use the obtained expressions from Sec. II in calculations to obtain the numerical results of Cd. In these calculations, using the Morse potential parameters $\alpha = 1.9069$ Å^{-1}, $D = 0.1675$ eV, and $r_0 = 3.0419$ Å [21], the atomic mass $m = 112.41$ u [36], and the lattice constants $a = 2.98$ Å, $c = 5.62$ Å, and $e = 1.89$ [36], we calculate and analyze the first four EXAFS cumulants $\sigma^{(1)}$, $\sigma^{(2)}$, $\sigma^{(3)}$ and $\sigma^{(4)}$, the correlated Debye temperature θ_D and frequency ω_D, the local force constants k_0, k_3 and k_4, and the logarithm of amplitude ratio $M(k,T)$ and phase difference $\Delta\Phi(k,T)$ of the anharmonic EXAFS oscillation.

Table 1. The thermodynamic parameters k_0, k_3, k_4, ω_D and θ_D of Cd obtained using the ACD model, the ACE [21] and CACE [22] models, and experimental Morse potential [21, 22].

Method	k_0(eVÅ^{-2})	k_3(eVÅ^{-3})	k_4(eVÅ^{-4})	ω_D ($\times 10^{13}$ Hz)	$\theta_D(K)$
ACD model with $e = 1.89$	2.975	1.429	1.521	3.186	243.391
ACD model with $e \approx \sqrt{8/3}$	3.045	1.452	1.534	3.224	246.275
ACE model [21]	3.045	1.452	-	3.224	246.275
CACE model [22]	3.045	1.452	1.534	3.224	246.275
Experimental Morse potential [21, 22]	3.001	1.429	1.509	3.199	244.447

The values of the correlated Debye temperature and frequency and local force constants , and of Cd are given in Table 1, in which our obtained results using the ACD model are calculated from Eqs. (9) and (11) in both cases e (for a distorted crystal) and e (for an undistorted crystal). Herein, the obtained results using the ACE [21] and CACE [22] models do not consider the structural distortion of Cd and use the structural parameter e in calculations. And the correlated Debye temperature and frequency can be inferred from the correlated Einstein temperature and frequency using the related expressions and [24, 29]. Meanwhile, the obtained results using the experimental Morse potential are calculated from Eqs. (9) and (11) based on the measured Morse parameters Å^{-1}, eV, and Å [21, 22]. It can be seen that our results fit with those obtained using the ACE and CACE models and experimental Morse potential [21, 22]. And our obtained results with e are the same as those obtained using the ACE and CACE models because Cd is considered an undistorted crystal in all these models. Moreover, compared to the values obtained from the experimental Morse potential, our obtained results with e fit better than those obtained using other models, as seen in Table 1. It means that the effect of structural distortion on the thermodynamic parameters of Cd needs to be considered in calculations.

The (a) first cumulant $\sigma^{(1)}(T)$, (b) second cumulant $\sigma^{(2)}(T)$, (c) third cumulant $\sigma^{(3)}(T)$, and (d) fourth EXAFS cumulant $\sigma^{(4)}(T)$ of Cd in the temperature dependence are shown in Fig. 2. Herein, our obtained results using the ACD model are calculated by Eqs. (12)-(18) in both cases

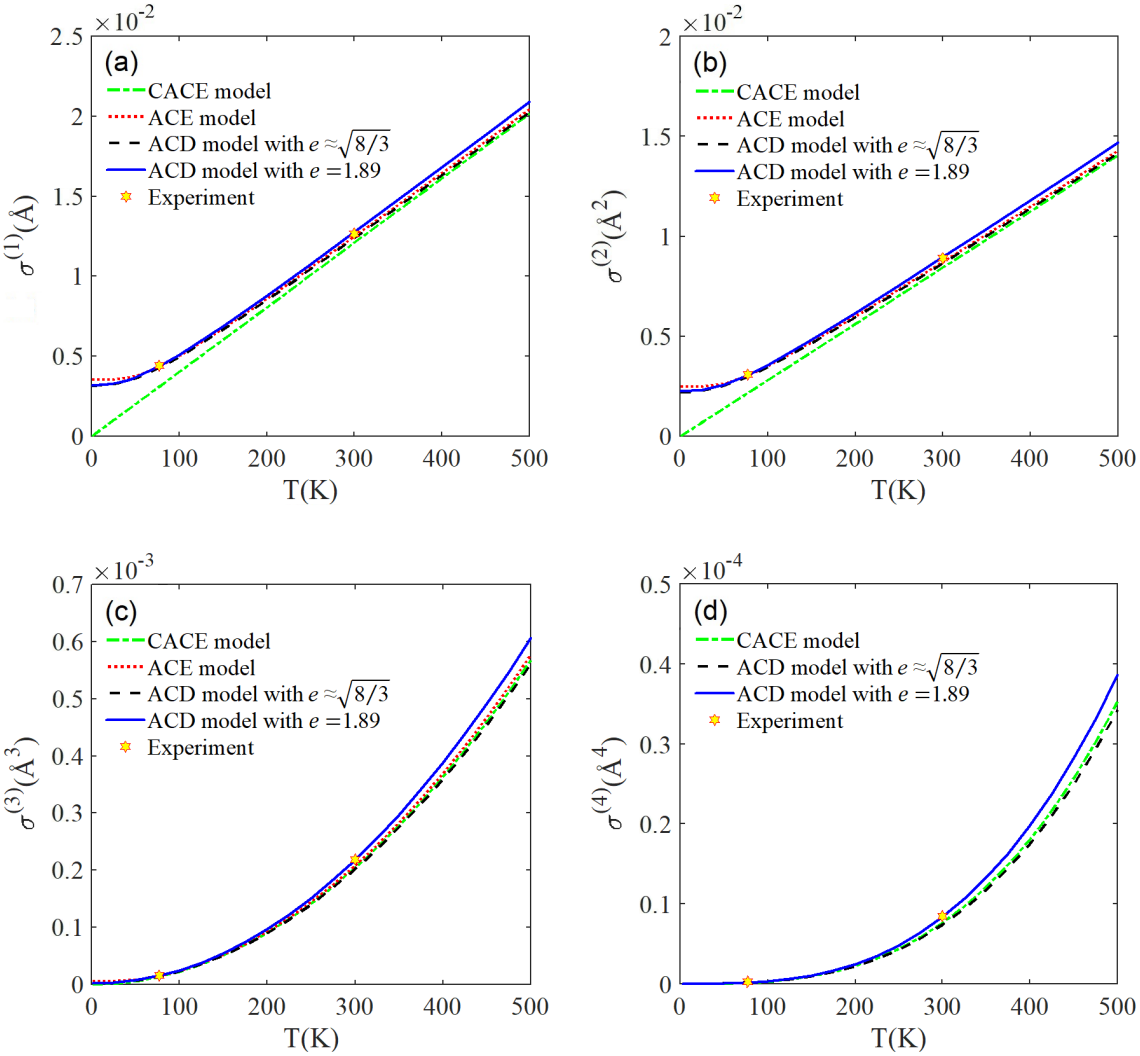

Fig. 2. Temperature-dependent (a) first, (b) second, (c) third, and (d) fourth EXAFS cumulants of Cd obtained using the ACD, ACE [21], CACE [22] models and experiments [22].

$e = 1.89$ (for a distorted crystal) and $e \approx \sqrt{8/3}$ (for an undistorted crystal), and the experimental values at 77 K and 300 K [22] are derived from measured EXAFS data analysis. Meanwhile, the ACE [21] and CACE [22] models only treat Cd as an undistorted crystal using a structural parameter $e \approx \sqrt{8/3}$, so the effect of structural distortion on the EXAFS cumulants of Cd is not taken into account in these models. It can be seen that our results fit well with those obtained from the ACE [21] and CACE (only in the high-temperature region) [22] models and experiment [22]. Also, in the LT region, the obtained results using the ACE model [21] are slightly greater than our calculated results because the ACE model use only one effective frequency to describe the atomic thermal vibrations. Meanwhile, the CACE model [22] approaches zero as the temperature

approaches the zero-point (ZP) because it cannot calculate the ZP energy and quantum effects using classical statistical theory. Moreover, our obtained results with e are significantly greater than our obtained results with $e \approx \sqrt{8/3}$ and fit best with the experimental data in comparison with other models, especially in the high-temperature (HT) region. It can be seen that the effect of structural distortion significantly increases the third and fourth cumulants (high-order cumulants) and visibly increases the first and second cumulants (low-order cumulants), as seen in Fig. 2.

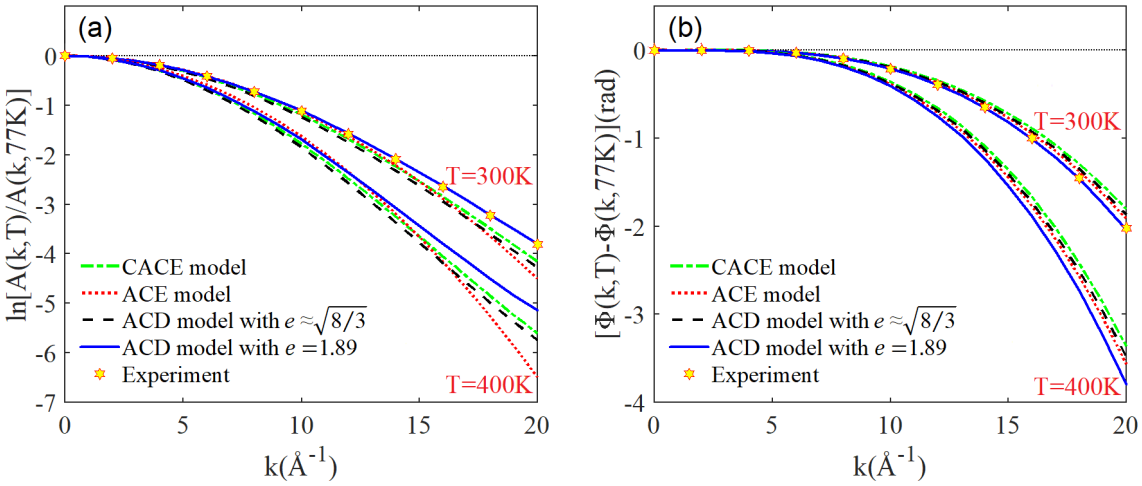

Fig. 3. Influence of temperature change on wavenumber-dependent (a) logarithm of amplitude ratios and (b) phase differences of Cd obtained using the ACD, ACE [21], CACE [22] models and experimental data [22] with the reference temperature K.

The wavenumber-dependent (a) logarithm of amplitude ratios $M(k,T) = \ln[\frac{A(k,T)}{A(k,77\text{K})}]$ and (b) phase differences $\Delta\Phi(k,T) = \Phi(k,T) - \Phi(k,77\ K)$ of Cd at $T = 300$ K, 400 K, and 500 K are shown in Fig. 3. The obtained results are calculated by Eqs. (4)-(5) with the temperature-dependent EXAFS cumulants are obtained using the ACD, ACE [21], and CACE [22] models and experiments. In these calculations, our obtained results using the ACD model are calculated in both cases e (for a distorted crystal) and e (for an undistorted crystal). It can be seen that our results have a reasonable characterization with those obtained using the ACE [21] and CACE [22] models. In comparison with these experimental values, the obtained results of using the ACE model [21] are not in good agreement because this model can not calculate the fourth EXAFS cumulants and treats it as zero. Meanwhile, the nonconformity of obtained results using the CACE model [22] is because this model does not work well in the LT region temperatures ($T_0 = 77$ K). Also, it can be seen that the influence of temperature strongly decreases the $\Delta W(k,T)$ and $\Delta\Phi(k,T)$, in which $\Delta W(k,T)$ decreases more slowly than $\Delta\Phi(k,T)$, especially at the large wavenumbers. Moreover, our obtained results with $e = 1.89$ are clearly different from our obtained results with $e \approx \sqrt{8/3}$ and fit best with those obtained using experimental data [22] in comparison with other models, especially for the phase differences. It can be seen that the effect of structural distortion visibly increases $M(k,T)$ and significantly decreases $\Delta\phi(k,t)$ with increasing the temperature T and wavenumber k, in which the effect of structural distortion on $M(k,t)$ changes faster and is smaller

than its effect on $\Delta\Phi(k,T)$, as seen in Fig. 3. It means that the EXAFS amplitude reduction is clearly reduced by the effect of structural distortion, and the EXAFS phase shift is significantly increased by this effect. Therefore, the structural distortion has a significant effect and needs to be considered in treating the temperature-dependent EXAFS oscillation, especially in the HT region.

IV. CONCLUSIONS

In this work, we have developed and expanded an efficient model for calculating and analyzing the temperature-dependent EXAFS oscillation of Cd with a distorted structure. The anharmonic EXAFS oscillation has been fully evaluated in variating the wavenumber using the analysis of the phase shift and amplitude reduction through the first four EXAFS cumulants. The temperature-dependent EXAFS cumulants are calculated by extending the ACD model that is based on the AE potential of Cd with a distorted structure. The effect of structural distortion is caused by the non-ideal axial ratio c/a of Cd described via a structural parameter e in the calculated expressions that can satisfy all fundamental properties in their temperature-dependence. The analytical results of the temperature-dependent EXAFS oscillation of Cd have indicated that the effect of structural distortion increases the logarithm of amplitude ratio and reduces the phase difference in variating the wavenumber. This effect is of considerable magnitude and should be considered in analyzing the temperature-dependent EXAFS signals of Cd, especially in the HT region.

The obtained numerical results using the present theoretical model satisfy well with those obtained using the experimental data and other models. This suitability indicates the efficiency of the present model in treating the temperature-dependent EXAFS oscillation of Cd with a distorted structure. This model can also efficiently treat the anharmonic EXAFS signals of other distorted crystalline metals with multiple acoustic phonons with low symmetry and isotropy in the temperature range from above zero to just before the melting point.

ACKNOWLEDGMENTS

The author would like to thank professor Nguyen Van Hung (Hanoi University of Science, Vietnam) for their helpful comments on the anharmonic EXAFS theory.

REFERENCES

[1] S. Shikata, K. Yamaguchi, A. Fujiwara, Y. Tamenori, K. Tsuruta, T. Yamada, S.S. Nicley, K. Haenen, S. Koizumi, *X-ray absorption near edge structure and extended X-ray absorption fine structure studies of P doped (111) diamond*, Diam. Relat. Mater. 105 (2020) 107769.

[2] P. Fornasini, R. Grisenti, M. Dapiaggi, and G. Agostini, *Local structural distortions in SnTe investigated by EXAFS*, *J. Phys.: Condens. Matter.* **33** (2021) 295404.

[3] T.S. Tien, Temperature-Dependent EXAFS Debye–Waller Factor of Distorted HCP Crystals, *J. Phys. Soc. Jpn.* **91** (2022) 054703.

[4] T. Yokoyama, K. Kobayashi, T. Ohta, and A. Ugawa, *Anharmonic interatomic potentials of diatomic and linear triatomic molecules studied by extended x-ray-absorption fine structure*, *Phys. Rev. B* **53** (1996) 6111. DOI: https://doi.org/10.1103/PhysRevB.53.6111

[5] T. S. Tien, *Effect of the non-ideal axial ratio c/a on anharmonic EXAFS oscillation of h.c.p. crystals*, *J. Synchrotron Rad.* **28** (2021) 1544.

[6] J. J. Rehr, F. D. Vila, J. J. Kas, N. Y. Hirshberg, K. Kowalski and B. Peng, *Equation of motion coupled-cluster cumulant approach for intrinsic losses in x-ray spectra*, *J. Chem. Phys.* **152** (2020) 174113.

[7] T. Yokoyama and S. Chaveanghong, *Anharmonicity in elastic constants and extended x-ray-absorption fine structure cumulants*, *Phys. Rev. Mater.* **3** (2019) 033607.

[8] R. B. Greegor and F. W. Lytle, *Extended x-ray absorption fine structure determination of thermal disorder in Cu: Comparison of theory and experiment*, *Phys. Rev. B* **20** (1979) 4902.
[9] G. Bunker, *Application of the ratio method of EXAFS analysis to disordered systems*, *Nucl. Instrum. Methods* **207** (1983) 437. DOI: https://doi.org/10.1016/0167-5087(83)90655-5
[10] J. J. Rehr and R. C. Albers, *Theoretical approaches to x-ray absorption fine structure*, *Rev. Mod. Phys.* **72** (2000) 621.
[11] M. Newville, *EXAFS analysis using FEFF and FEFFIT*, *J. Synchrotron Rad.* **8** (2001) 96.
[12] M. Newville, B. Ravel, D. Haskel, J. J. Rehr, E. A. Stern, and Y. Yacoby, *Analysis of multiple-scattering XAFS data using theoretical standards*, *Physica B* **208-209** (1995) 154.
[13] A. L. Ankudinov, B. Ravel, J. J. Rehr and S. D. Conradson, *Real-space multiple-scattering calculation and interpretation of x-ray-absorption near-edge structure*, *Phys. Rev. B* **58** (1998) 7565.
[14] S. I. Zabinsky, J. J. Rehr, A. Ankudinov, R. C. Albers and M. J. Eller, *Multiple-scattering calculations of x-ray-absorption spectra*, *Phys. Rev. B* **52** (1995) 2995.
[15] J. J. Rehr, J. Mustre de Leon, S. I. Zabinsky and R. C. Albers, *Theoretical x-ray absorption fine structure standards*, *J. Am. Chem. Soc.* **113** (1991) 5135.
[16] T. S. Tien, *Investigation of the anharmonic EXAFS oscillation of distorted HCP crystals based on extending quantum anharmonic correlated Einstein model*, *Jpn. J. Appl. Phys.* **60** (2021) 112001.
[17] G. Buxbaum and G. Pfaff, Industrial Inorganic Pigments, 3rd ed., Wiley-VCH, New York (2005).
[18] M. Hou, L. Li and M. Zhuang, *Research on application mechanism of cadmium in new energy vehicle charging group*, *IOP Conf. Ser.: Earth Environ. Sci.* **227** (2019) 052046.
[19] A. M. Kadim, Applications of Cadmium Telluride (CdTe) in Nanotechnology, IntechOpen, London (2019).
[20] N. E. Galushkin, N. N. Yazvinskaya and D. N. Galushkin, *Nickel-cadmium batteries with pocket electrodes as hydrogen energy storage units of high-capacity*, *J. Energy Storage* **39** (2021) 102597.
[21] N. V. Hung, L. H. Hung, T. S. Tien and R. R. Frahm, *Anharmonic effective potential, local force constant and EXAFS of HCP crystals: Theory and comparison to experiment*, *Int. J. Mod. Phys. B* **22** (2008) 5155.
[22] N. V. Hung, T. S. Tien, N. B. Duc and D. Q. Vuong, *High-order expanded XAFS Debye Waller factors of HCP crystals based on classical anharmonic correlated Einstein model*, *Mod. Phys. Lett. B* **28** (2014) 1450174.
[23] N. V. Hung, N. B. Trung and B. Kirchner, *Anharmonic correlated Debye model Debye–Waller factors*, *Physica B* **405** (2010) 2519.
[24] N. B. Duc, N. V. Hung, H. D. Khoa, D. Q. Vuong and T. S. Tien, *Thermodynamic properties and anharmonic effects in XAFS based on anharmonic correlated debye model Debye–Waller factors*, *Adv. Mater. Sci. Eng.* **2018** (2018) 3263170.
[25] N. B. Duc, V. Q. Tho, T. S. Tien, D. Q. Khoa, and H. K. Hieu, *Pressure and temperature dependence of EXAFS Debye-Waller factor of platinum*, *Radiat. Phys. Chem.* **149** (2018) 61.
[26] T. S. Tien, *Analysis of EXAFS oscillation of monocrystalline diamond-semiconductors using anharmonic correlated Debye model*, *Eur. Phys. J. Plus.* **136** (2021) 539.
[27] E. D. Crozier, J. J. Rehr, and R. Ingalls, X-ray Absorption: Principles, Applications, Techniques of EXAFS, SEXAFS, XANES, edited by D. C. Koningsberger and R. Prins, Chap. 9, Wiley, New York (1988).
[28] T. S. Tien, *Advances in studies of the temperature dependence of the EXAFS amplitude and phase of FCC crystals*, *J. Phys. D: Appl. Phys.* **53** (2020) 315303.
[29] N. V. Hung, T. S. Tien and L. H. Hung, *High-order anharmonic effective potentials and EXAFS cumulants of FCC crystals calculated from a Morse interaction potential*, *Comm. in Phys.* **18** (2008) 75.
[30] L. Tröger, T. Yokoyama, D. Arvanitis, T. Lederer, M. Tischer and K. Baberschke, *Determination of bond lengths, atomic mean-square relative displacements, and local thermal expansion by means of soft-x-ray photoabsorption*, *Phys. Rev. B* 49 (1994) 888.
[31] A. Sanson, *On the neglecting of higher-order cumulants in EXAFS data analysis*, *J. Synchrotron Radiat.* **16** (2009) 864.
[32] P. Fornasini, R. Grisenti, M. Dapiaggi, G. Agostini and T. Miyanaga, *Nearest-neighbour distribution of distances in crystals from extended X-ray absorption fine structure*, *J. Chem. Phys.* 147 (2017) 044503.
[33] P. M. Morse, *Diatomic molecules according to the wave mechanics. II. Vibrational levels*, *Phys. Rev.* **34** (1929) 57.

[34] L. A. Girifalco and V. G. Weizer, *Application of the Morse potential function to cubic metals*, *Phys. Rev.* **114** (1959) 687.

[35] N. V. Hung and J. J. Rehr, *Anharmonic correlated Einstein-model Debye-Waller factors*, *Phys. Rev. B* 56 (1997) 43.

[36] P. Enghag, *Encyclopedia of the elements: Technical data, history, processing, applications*, Wiley-VCH, Weinheim (2004).